Copyright Notice

Posterior Cramér-Rao Bound and Suboptimal Filtering for IMU/GNSS based Cooperative Train Localization

Benjamin Siebler and Stephan Sand
German Aerospace Center (DLR)
Institute of Communications and Navigation
Wessling, Germany
Email: {benjamin.siebler,stephan.sand}@dlr.de

***Abstract*—The optimal estimator for the hidden state of nonlinear systems is often not known or it is computational unfeasible. In this situation suboptimal algorithms must be used. An important performance metric for these algorithms is the difference of their root mean square error (RMSE) compared to the RMSE of the optimal estimator. If the optimal estimator is unknown it is useful to have a lower bound for the RMSE. Such a bound is defined by the posterior Cramér-Rao lower bound (PCRB) which is also valid for biased estimators. In this paper a version of the PCRB for nonlinear systems considering known inputs is applied to analyze the performance of an extended Kalman filter (EKF) and unscented Kalman filter (UKF) for GNSS/IMU based cooperative train localization. The analysis is realized by performing a simulation study for different track and satellite geometries. After an initial phase with larger errors both, the EKF and UKF are able to estimate the bias on the pseudoranges and the receiver clocks and they attain the PCRB.**

I. INTRODUCTION

The localization of trains at its current state is based mainly on infrastructure components like balises and magnetic axle counters. This is sufficient for the current rail management systems which allow trains only to drive with the absolute braking distance between them. However, this approach prohibits real-time localization and does not utilize the available capacity of the track network. In future, automated railway systems reliable and accurate localization systems will be indispensable. For reliable localization of trains, it can be exploited that the movement of the trains is limited by strong constrains forced on them by the track. Taking this into account the 3D localization can be reduced to the one dimensional arc length the train has driven on a certain part of the track network. For absolute positioning with global navigation satellite systems (GNSS) then only two satellites are needed for estimating the train position and the user clock error. This approach assumes that a digital map of the track network exists, that links the 1D position to a global 3D coordinate system.

In the literature, several localization systems were developed that provide train position in real-time. The sensors used in most of these systems include inertial measurement units (IMU) and GNSS. There are also some unconventional approaches using active eddy current sensors [1] or passive magnetic sensors and pattern recognition techniques to extract speed and position information from the earth magnetic field distorted by the railway infrastructure [2]. In addition, Heirich et al. developed a simultaneous localization and mapping (SLAM) algorithm for railways, which is able to create feature rich maps of the track network [3].

In this paper the cooperative approach presented in [4] is used. The assumption in [4] is that multiple trains cooperate with each other by sharing their GNSS and IMU measurements and that a map of the track network is available. The shared measurements are processed in a centralized localization filter and the 1D train positions are estimated jointly. The resulting estimation problem is nonlinear due to the map and the GNSS pseudorange measurement model. Therefore the optimal estimator for the train positions is unknown and a suboptimal algorithm must be used. To still achieve a good position accuracy care must be taken when choosing the suboptimal algorithm. A widely used method to evaluate the performance of suboptimal filters is to derive a lower bound for the mean square error (MSE) matrix. If the filter reaches this bound it is efficient and no better estimator with respect to the MSE matrix can be found. To calculate this bound for the proposed joint localization filter the posterior Cramér-Rao bound depending on a known input, here the acceleration measured by an IMU, is derived. The advantage of including an input in the PCRB is that the trajectories of the trains, used in the calculation of the PCRB, can be controlled. This issue will be addressed in more detail in section II-B.

After the bound is derived in section II and III the state space model is introduced in section IV. The PCRB for the concrete estimation problem is stated in V and evaluated in an simulation study in section VI. In the simulation study different track geometries and velocity trajectories are considered to verify their influence on the accuracy. In section VII the results of the simulations are presented followed by the conclusion in VIII.

II. POSTERIOR CRAMÉR-RAO BOUND

A. Standard version of the PCRB

The posterior Cramér-Rao bound is a method to evaluate the performance of Bayesian estimators and was first derived by van Trees [5]. It differs from the classical Cramér-Rao bound by considering a random parameter or state vector $\mathbf{x}$ with the dimension $N_{\mathbf{x}}$ and the probability density function (pdf) $p(\mathbf{x})$. The PCRB has the advantage, that it is no longer necessary to show the unbiasedness of the estimator for the bound to be valid. The bound is defined by the inequality

$$E_{\mathbf{x},\mathbf{y}}\{(\hat{\mathbf{x}}-\mathbf{x})(\hat{\mathbf{x}}-\mathbf{x})^T\} = \mathbf{M} \geq \mathbf{J}^{-1} \tag{1}$$

and the Bayesian information matrix (BIM)

$$\mathbf{J} = E_{\mathbf{x},\mathbf{y}}\{-\Delta_{\mathbf{x}}^{\mathbf{x}} \log p(\mathbf{x},\mathbf{y})\} \tag{2}$$

with the operator

$$\Delta_{\mathbf{b}}^{\mathbf{a}} = \nabla_{\mathbf{b}} \nabla_{\mathbf{a}}^{T} \quad \text{and} \quad \nabla_{\mathbf{x}} = \begin{bmatrix} \frac{\partial}{\partial x_1} & \cdots & \frac{\partial}{\partial x_N} \end{bmatrix}^{T} \tag{3}$$

and the $N_{\mathbf{y}}$ dimensional observation vector $\mathbf{y}$. The expectation is with respect to the joint pdf of $\mathbf{x}$ and $\mathbf{y}$ as indicated by the indices of the expectation operator. The inequality in (1) states that the difference between the mean square error (MSE) matrix $\mathbf{M}$ and the inverse of the BIM is a semipositive-definite matrix and that for the diagonal elements of $\mathbf{M}$ the following inequality holds

$$\sqrt{\mathbf{M}_{i,i}} \geq \sqrt{\mathbf{J}_{i,i}^{-1}}. \tag{4}$$

Therefore the root mean square error (RMSE) of a single element in $\mathbf{x}$ is always greater than or equal to the square root of the according element of the inverse BIM. With a simple reformulation of (2), a connection to the classical bound can be made by dividing the BIM in an observation depending part $\mathbf{J}_{\mathrm{D}}$ and a part dependent on the a priori knowledge $\mathbf{J}_{\mathrm{P}}$ given by the pdf $p(\mathbf{x})$

$$\begin{aligned} \mathbf{J} &= E_{\mathbf{x},\mathbf{y}}\{-\Delta_{\mathbf{x}}^{\mathbf{x}} \log p(\mathbf{y}|\mathbf{x})\} + E_{\mathbf{x}}\{-\Delta_{\mathbf{x}}^{\mathbf{x}} \log p(\mathbf{x})\} \\ &= \mathbf{J}_{\mathrm{D}} + \mathbf{J}_{\mathrm{P}}. \end{aligned} \tag{5}$$

This is the result when the joint pdf of the state and the observations $p(\mathbf{x},\mathbf{y})$ in (2) is replaced by the relation $p(\mathbf{y}|\mathbf{x})p(\mathbf{x})$. The data dependent part can be rewritten as expectation of the Fisher information matrix (FIM) with respect to the pdf $p(\mathbf{x})$ of the parameter vector $\mathbf{J}_{\mathrm{D}} = E_{\mathbf{x}}\{\mathbf{J}_{\mathrm{F}}(\mathbf{x})\}$. For the PCRB to hold the derivations and expectations in (2) must exist and

$$\lim_{x_j \to \pm\infty} B_i(\mathbf{x}) p(\mathbf{x}) = 0 \quad \forall j \in \{1, \ldots, N_{\mathbf{x}}\} \tag{6}$$

must be fulfilled for each element B_i of the estimator bias

$$\mathbf{B}(\mathbf{x}) = \int_{\mathbb{R}^{N_{\mathbf{y}}}} [\hat{\mathbf{x}} - \mathbf{x}] p(\mathbf{y}|\mathbf{x}) d\mathbf{y}. \tag{7}$$

B. PCRB conditioned on input vector

For the evaluation of the suboptimal filters for cooperative train localization, a PCRB under the condition of a known input is derived. This is done to simplify the approximation of the bound with Monte Carlo methods and to gain a better control of the simulated scenarios. In the state space model introduced in section IV this input is the acceleration of the train measured with an IMU. In the normal PCRB, the acceleration has to be included in the state vector and the accelerometer measurements are part of the observation vector $\mathbf{y}$. This makes the Monte Carlo simulation difficult because it has to approximate the expectation in (2) for the whole state space. This increases the number of Monte Carlo runs needed to get close to the true value. Another problem is that considering the complete state space, and thereby all possible acceleration trajectories, obscures the information about a specific trajectory. Especially in the railway domain this is unwanted because the trains follow strict patterns. The introduction of the acceleration as input avoids this problem by making the train movement controllable. Because we can now focus on specific acceleration trajectories the number of Monte Carlo runs needed to approximate the PCRB can be reduced and only the wanted information is included.

Theorem 1. *For the MSE of an estimator conditioned on* $\mathbf{u}$ *the following inequality holds*

$$\mathbf{M}_{\mathrm{u}} = E_{\mathbf{x},\mathbf{y}|\mathbf{u}}\{(\hat{\mathbf{x}} - \mathbf{x})(\hat{\mathbf{x}} - \mathbf{x})^{T}\} \geq \mathbf{J}_{\mathrm{u}}^{-1} \tag{8}$$

$$\mathbf{J}_{\mathrm{u}} = E_{\mathbf{x},\mathbf{y}|\mathbf{u}}\{-\Delta_{\mathbf{x}}^{\mathbf{x}} \log p(\mathbf{x},\mathbf{y}|\mathbf{u})\} \tag{9}$$

when for each elements B_i *of the estimator bias*

$$\mathbf{B}(\mathbf{x},\mathbf{u}) = \int_{\mathbb{R}^{N_{\mathbf{y}}}} (\hat{\mathbf{x}} - \mathbf{x}) p(\mathbf{y}|\mathbf{x},\mathbf{u}) d\mathbf{y} \tag{10}$$

the relation

$$\lim_{x_j \to \pm\infty} B_i(\mathbf{x},\mathbf{u}) p(\mathbf{x}|\mathbf{u}) = 0 \quad \forall j \in \{1, \ldots, N_{\mathbf{x}}\} \tag{11}$$

is fulfilled and the derivations and expectations in (8) exist.

Proof: The proof follows the approach for the standard PCRB from [6] but the starting point is now the equation of the estimation bias given by (10). Multiplying (10) with $p(\mathbf{x}|\mathbf{u})$ and taking the derivate with respect to $\mathbf{x}$, and then integrating it over the domain of $\mathbf{x}$ gives

$$\int_{\mathbb{R}^{N_{\mathbf{x}}}} \nabla_{\mathbf{x}} \big(\mathbf{B}(\mathbf{x},\mathbf{u})^{T} p(\mathbf{x}|\mathbf{u})\big) d\mathbf{x} = \nabla_{\mathbf{x}} \int_{\mathbb{R}^{N_{\mathbf{y}}+N_{\mathbf{x}}}} (\hat{\mathbf{x}} - \mathbf{x})^{T} p(\mathbf{x},\mathbf{y}|\mathbf{u}) d\mathbf{x} d\mathbf{y}. \tag{12}$$

With condition (11) the left hand side of the equation becomes the zero matrix $\mathbf{0}$ and the right hand side can be rewritten to

$$\mathbf{0} = -\mathbf{I} + \int_{\mathbb{R}^{N_{\mathbf{y}}+N_{\mathbf{x}}}} \nabla_{\mathbf{x}} p(\mathbf{x},\mathbf{y}|\mathbf{u}) (\hat{\mathbf{x}} - \mathbf{x})^{T} d\mathbf{x} d\mathbf{y} \tag{13}$$

this results in

$$\begin{aligned} \mathbf{I} &= \int_{\mathbb{R}^{N_{\mathbf{x}}+N_{\mathbf{y}}}} \nabla_{\mathbf{x}} (\log p(\mathbf{x},\mathbf{y}|\mathbf{u})) (\hat{\mathbf{x}} - \mathbf{x})^{T} p(\mathbf{x},\mathbf{y}|\mathbf{u}) d\mathbf{x} d\mathbf{y} \\ &= E_{\mathbf{x},\mathbf{y}|\mathbf{u}}\{\nabla_{\mathbf{x}} (\log p(\mathbf{x},\mathbf{y}|\mathbf{u})) (\hat{\mathbf{x}} - \mathbf{x})^{T}\} \end{aligned} \tag{14}$$

with the identity matrix $\mathbf{I}$. Constructing the autocorrelation matrix for the vector $\begin{bmatrix} (\hat{\mathbf{x}} - \mathbf{x}) & \nabla_{\mathbf{x}} \log p(\mathbf{x},\mathbf{y}|\mathbf{u}) \end{bmatrix}^{T}$ and inserting (8), (9) and (14) results in the block matrix

$$E_{\mathbf{x},\mathbf{y}|\mathbf{u}}\left\{ \begin{bmatrix} \hat{\mathbf{x}} - \mathbf{x} \\ \nabla_{\mathbf{x}} \log p(\mathbf{x},\mathbf{y}|\mathbf{u}) \end{bmatrix} \begin{bmatrix} \hat{\mathbf{x}} - \mathbf{x} \\ \nabla_{\mathbf{x}} \log p(\mathbf{x},\mathbf{y}|\mathbf{u}) \end{bmatrix}^{T} \right\} = \begin{bmatrix} \mathbf{M}_{\mathrm{u}} & \mathbf{I} \\ \mathbf{I} & \mathbf{J}_{\mathrm{u}} \end{bmatrix}. \tag{15}$$

The correlation matrix (15) is semipositive-definite and symmetric. This is also true for the Schure complement

$$\mathbf{S} = \mathbf{M}_{\mathrm{u}} - \mathbf{J}_{\mathrm{u}}^{-1} \tag{16}$$

when $\mathbf{J}_{\mathrm{u}}$ is positive definite. This introduces no additional constraint because $\mathbf{J}_u$ is semipositive-definite by default and to be invertible all eigenvalues must be positive. This leads to the proposed inequality

$$\mathbf{M}_{\mathbf{u}} - \mathbf{J}_{\mathrm{u}}^{-1} \geq \mathbf{0}. \tag{17}$$

■

The derived bound is a special case of the hybrid parameter bound in [7]. In the hybrid bound the parameter vector contains random and nonrandom parameters. The bound is defined only for the random parameters under the assumption that the rest is known. If the input variables are considered as nonrandom parameters the hybrid bound is equal to (9).

III. Recursive Calculation of the PCRB

For the performance evaluation of a filter for the nonlinear dynamic system

$$\mathbf{x}_{k+1} = \mathbf{f}(\mathbf{x}_k, \mathbf{u}_k, \mathbf{n}_k) \tag{18}$$

$$\mathbf{y}_k = \mathbf{h}(\mathbf{x}_k, \mathbf{w}_k) \tag{19}$$

with process and measurement noise $\mathbf{n}_k$ and $\mathbf{w}_k$, the bound must be known for each measurement epoch k. This can be done by calculating the bound for a combined state vector $\mathbf{X}_k = [\mathbf{x}_0^T, \ldots, \mathbf{x}_k^T]^T$ and the vector of all measurements $\mathbf{Y}_k = [\mathbf{y}_0^T, \ldots, \mathbf{y}_k^T]^T$ and inputs $\mathbf{U}_k = [\mathbf{u}_0^T, \ldots, \mathbf{u}_k^T]^T$ up to time step k. This leads to a growing BIM in each time step. To limit the size to the state dimension the authors in [8] propose a recursive version of the bound by exploiting the structure of the BIM for the combined vector $[\mathbf{X}_k^T, \mathbf{x}_{k+1}^T]^T$

$$\mathbf{J}_{k+1} = \mathbf{D}_k^{22} - \mathbf{D}_k^{21}(\mathbf{J}_k + \mathbf{D}_k^{11})^{-1}\mathbf{D}_k^{12} \tag{20}$$

with

$$\mathbf{D}_k^{11} = E_{\mathbf{x}_k, \mathbf{x}_{k+1}}\{-\Delta_{\mathbf{x}_k}^{\mathbf{x}_k} \log p(\mathbf{x}_{k+1}|\mathbf{x}_k)\} \tag{21}$$

$$\mathbf{D}_k^{12} = E_{\mathbf{x}_k, \mathbf{x}_{k+1}}\{-\Delta_{\mathbf{x}_k}^{\mathbf{x}_{k+1}} \log p(\mathbf{x}_{k+1}|\mathbf{x}_k)\} = \mathbf{D}_k^{21,T} \tag{22}$$

$$\begin{aligned}\mathbf{D}_k^{22} =& E_{\mathbf{x}_k, \mathbf{x}_{k+1}}\{-\Delta_{\mathbf{x}_{k+1}}^{\mathbf{x}_{k+1}} \log p(\mathbf{x}_{k+1}|\mathbf{x}_k)\} + \\ & E_{\mathbf{x}_{k+1}, \mathbf{y}_{k+1}}\{-\Delta_{\mathbf{x}_{k+1}}^{\mathbf{x}_{k+1}} \log p(\mathbf{y}_{k+1}|\mathbf{x}_{k+1})\}.\end{aligned} \tag{23}$$

In the derivation, the Markov property of the system in (18) was used to limit the dependency of $p(\mathbf{x}_{k+1}|\mathbf{x}_k)$ to $\mathbf{x}_k$ and not on the complete state history. For the input version the recursive formulation can be easily found by applying the steps from [8] on (8) and (9)

$$\mathbf{J}_{\mathrm{u},k+1} = \mathbf{D}_{\mathrm{u},k}^{22} - \mathbf{D}_{\mathrm{u},k}^{21}(\mathbf{J}_{\mathrm{u},k} + \mathbf{D}_{\mathrm{u},k}^{11})^{-1}\mathbf{D}_{\mathrm{u},k}^{12} \tag{24}$$

with

$$\mathbf{D}_{\mathrm{u},k}^{11} = E_{\mathbf{x}_k, \mathbf{x}_{k+1}|\mathbf{U}_k}\{-\Delta_{\mathbf{x}_k}^{\mathbf{x}_k} \log p(\mathbf{x}_{k+1}|\mathbf{x}_k, \mathbf{u}_k)\} \tag{25}$$

$$\mathbf{D}_{\mathrm{u},k}^{12} = E_{\mathbf{x}_k, \mathbf{x}_{k+1}|\mathbf{U}_k}\{-\Delta_{\mathbf{x}_k}^{\mathbf{x}_{k+1}} \log p(\mathbf{x}_{k+1}|\mathbf{x}_k, \mathbf{u}_k)\} \tag{26}$$

$$\begin{aligned}\mathbf{D}_{\mathrm{u},k}^{22} =& E_{\mathbf{x}_k, \mathbf{x}_{k+1}|\mathbf{U}_k}\{-\Delta_{\mathbf{x}_{k+1}}^{\mathbf{x}_{k+1}} \log p(\mathbf{x}_{k+1}|\mathbf{x}_k, \mathbf{u}_k)\} + \\ & E_{\mathbf{x}_{k+1}, \mathbf{y}_{k+1}|\mathbf{U}_k}\{-\Delta_{\mathbf{x}_{k+1}}^{\mathbf{x}_{k+1}} \log p(\mathbf{y}_{k+1}|\mathbf{x}_{k+1})\}.\end{aligned} \tag{27}$$

This is basically the same as in (20)–(23), the only difference is that the expectations and pdf's are conditioned on the history $\mathbf{U}_k$ of the input vector.

IV. State Space model

The state space model for the cooperative localization filter is composed of the kinematic state describing the movement of each train and parts describing the pseudorange, receiver clock and accelerometer errors.

A. Kinematic train state and accelerometer errors

The movement of the train is described by a two dimensional vector containing the 1D position s and velocity $\dot{s}$. The acceleration a of the train is not part of the state vector, instead it is used as input. The input is assumed to be measured by an accelerometer in driving direction. To take into account the typical accelerometer errors we include for train i a sensor bias $b_{\mathrm{a},i}$ in the state and add the measurement noise as process noise $n_{\mathrm{a},i}$ to the differential equation of the velocity. The sensor bias is assumed to be a first order Gauss-Markov process with the driving noise $n_{\mathrm{ba},i}$ and time constant $\tau_{\mathrm{b},i}$. The kinematic state of train i is therefore defined by

$$\mathbf{D}_i = [s_i, \dot{s}_i, b_{\mathrm{a},i}]^T \tag{28}$$

and the system of differential equations

$$\frac{d}{dt}\begin{bmatrix} s \\ \dot{s} \\ b_{\mathrm{a},i} \end{bmatrix} = \begin{bmatrix} 0 & 1 & 0 \\ 0 & 0 & -1 \\ 0 & 0 & \frac{1}{\tau_{\mathrm{b},i}} \end{bmatrix}\begin{bmatrix} s \\ \dot{s} \\ b_{\mathrm{a},i} \end{bmatrix} + \begin{bmatrix} 0 \\ 1 \\ 0 \end{bmatrix} a_i + \begin{bmatrix} 0 & 0 \\ 1 & 0 \\ 0 & 1 \end{bmatrix}\begin{bmatrix} n_{\mathrm{a},i} \\ n_{\mathrm{ba},i} \end{bmatrix}. \tag{29}$$

For the ease of implementation it is assumed in (29) that the trains move on a plain parallel to the earth's surface. If this condition does not hold the measured acceleration must be compensated for gravity and the attitude must be estimated.

B. Receiver clock error

The receiver clock error is characterized by the vector

$$\mathbf{C}_i = \left[\delta t_i, \delta \dot{t}_i\right]^T \tag{30}$$

with clock error δt and clock drift $\delta \dot{t}$. An adequate representation of the temporal behavior is a second order random walk as proposed in [9]

$$\frac{d}{dt}\begin{bmatrix} \delta t_i \\ \delta \dot{t}_i \end{bmatrix} = \begin{bmatrix} 0 & 1 \\ 0 & 0 \end{bmatrix}\begin{bmatrix} \delta t_i \\ \delta \dot{t}_i \end{bmatrix} + \begin{bmatrix} n_{\delta t,i} \\ n_{\delta \dot{t},i} \end{bmatrix}. \tag{31}$$

In (31), $[n_{\delta t,i},\ n_{\delta \dot{t},i}]^T$ is a white Gaussian driving noise.

C. Pseudorange bias

Errors that depend mainly on the satellite but not on the receiver are captured by a bias ν^j for each satellite j. The errors that can be seen as a receiver independent bias are e.g. the tropospheric and ionospheric errors when the different receivers are located in an area of a few square kilometers. The evolution of this bias is approximated with a first order random walk process

$$\frac{d}{dt}\nu^j = n_{\nu^j} \tag{32}$$

with the driving noise n_{ν^j}. Collecting the bias for N_{S} satellites in a vector we get the pseudorange bias state $\mathbf{N}$

$$\mathbf{N} = \left[\nu^1, \ldots, \nu^{N_{\mathrm{S}}}\right] \tag{33}$$

D. Complete state vector

The final state vector $\mathbf{x}$ is a combination of the above mentioned parts. The dimension of the state is $5 \cdot N_{\mathrm{T}} + N_{\mathrm{S}}$, depending on the number of trains N_{T} considered in the filter.

$$\mathbf{x} = \begin{bmatrix} \mathbf{D}_1 & \mathbf{C}_1 & \cdots & \mathbf{D}_{N_T} & \mathbf{C}_{N_T} & \mathbf{N} \end{bmatrix}^T \tag{34}$$

E. Measurement model

Due to the introduction of the satellite dependent pseudo-range bias ν^j in (33), the measurement model for receiver i and satellite j can be written as

$$\rho_i^j = ||\mathbf{m}(s_i) - \mathbf{x}^j|| + c\delta t_i - \nu^j + w_i. \tag{35}$$

With the speed of light c, the receiver noise w_i and the mapping function $\mathbf{m}(\cdot)$. The mapping $\mathbf{m}$ is needed to link the satellite position $\mathbf{x}^j$ given in an global ECEF coordinate system to the local 1D coordinate system of the rail tracks. In addition to the Euclidian norm $||\cdot||$ the map introduces an nonlinearity that must be handled in the estimation process.

The complete measurement model is obtained by collecting the measurements from all N_T receivers in a vector

$$\left[\rho_1^1 \ \cdots \ \rho_1^{N_S} \ \cdots \ \rho_{N_T}^1 \cdots \rho_{N_T}^{N_S}\right]^T = \mathbf{y}_k = \mathbf{h}(\mathbf{x}_k, \mathbf{w}_k). \tag{36}$$

V. PCRB for Cooperative Train Localization

The state space model in section IV has a linear system equation and a nonlinear measurement equation and the noise is assumed to be additive white Gaussian noise (AWGN). With the process noise gain matrix $\mathbf{G}$ the system can be written as

$$\mathbf{x}_{k+1} = \mathbf{F}_k\mathbf{x}_k + \mathbf{B}\mathbf{u}_k + \mathbf{G}_k\mathbf{n}_k \tag{37}$$

$$\mathbf{y}_k = \mathbf{h}(\mathbf{x}_k) + \mathbf{w}_k. \tag{38}$$

For such systems, the pdf $p(\mathbf{x}_{k+1}|\mathbf{x}_k)$ and $p(\mathbf{y}_{k+1}|\mathbf{x}_{k+1})$ can be found from the pdf of the noise terms $\mathbf{n}_k \sim \mathcal{N}(\mathbf{0}, \mathbf{Q})$ and $\mathbf{w}_k \sim \mathcal{N}(\mathbf{0}, \mathbf{R})$ and the system equations (37)–(38). Inserting this into equation (25)–(27) results in the concrete formulation of the PCRB

$$\mathbf{D}_k^{11} = \mathbf{F}_k^T(\mathbf{G}_k\mathbf{Q}_k\mathbf{G}_k^T)^{-1}\mathbf{F}_K \tag{39}$$

$$\mathbf{D}_k^{12} = -\mathbf{F}_k^T(\mathbf{G}_k\mathbf{Q}_k\mathbf{G}_k^T)^{-1} = \mathbf{D}_k^{21,T} \tag{40}$$

$$\mathbf{D}_k^{22} = E_{\mathbf{x}_{n+1}|\mathbf{U}_k}\{\tilde{\mathbf{h}}(\mathbf{x}_{k+1})\mathbf{R}_k^{-1}\tilde{\mathbf{h}}(\mathbf{x}_{k+1})^T\} + (\mathbf{G}_k\mathbf{Q}_k\mathbf{G}_k^T)^{-1} \tag{41}$$

with

$$\tilde{\mathbf{h}}(\mathbf{x}_{k+1}) = \nabla_{\mathbf{x}_{k+1}}\mathbf{h}^T(\mathbf{x}_{k+1}). \tag{42}$$

VI. Simulation Parameters and Scenarios

To evaluate the EKF and UKF for the system in section IV a simulation study is performed. In this study, two trains are simulated, first driving on a straight track and then entering a curve after 300 m with a radius of $R = 1000$ m. The bound and the filters are evaluated for uniform and accelerated movement of the trains. In the uniform case, one train moves with constant velocity of $25\,\mathrm{m\,s^{-1}}$ and one is standing on the straight track. For the accelerated scenario one train drives with constant velocity of $30\,\mathrm{m\,s^{-1}}$ and the other one starts with $20\,\mathrm{m\,s^{-1}}$ and then accelerates with $0.3\,\mathrm{m\,s^{-2}}$. With this acceleration the second train approaches the leading train until they meet after approximately 66 s. The starting point of the trains in both scenarios is the beginning of the straight track.

The standard deviations for the process and measurement noise are: $\sigma_{n_{\mathrm{a},i}} = 2 \times 10^{-3}\,\mathrm{m\,s^{-2}}$, $\sigma_{n_{\mathrm{ba},i}} = 1 \times 10^{-5}\,\mathrm{m\,s^{-3}}$, $\sigma_{n_{\delta t,i}} = 0.375\,\mathrm{m\,s^{-1}}$, $\sigma_{n_{\delta i,i}} = 0.189\,\mathrm{m\,s^{-2}}$, $\sigma_{n_{\nu j}} = 0.1\,\mathrm{m\,s^{-1}}$ and $\sigma_w = 1$ m. For each scenario, the simulation was performed for four static satellite constellations. The number of visible satellites in these constellations is four and eight. To show the impact of the geometry two different geometric dilution of precision (GDOP) values are used. The filter state is initialized randomly according to the initial state covariance matrix $\mathbf{P}_0$ and the mean $\mathbf{x}_0$. The value of $\mathbf{x}_0$ is zero except for the velocities which are set to fit the uniform and accelerated scenario i.e. for the first train $25\,\mathrm{m\,s^{-1}}$ and $30\,\mathrm{m\,s^{-1}}$ and for the second train $0\,\mathrm{m\,s^{-1}}$ and $20\,\mathrm{m\,s^{-1}}$. To calculate the PCRB and filter RMSE multiple Monte Carlo runs must be performed. In each run, the system equations from section IV are simulated for 60 s with different samples of the process noise. With this the expectation in (41) can be approximated. To estimate the MSE matrix in (8) for the EKF and UKF also the measurement noise has to be sampled for each run. This leads to a rapidly growing complexity with each additional run. We strike here a compromise between computation time and accuracy and choose to simulate 1000 Monte Carlo runs

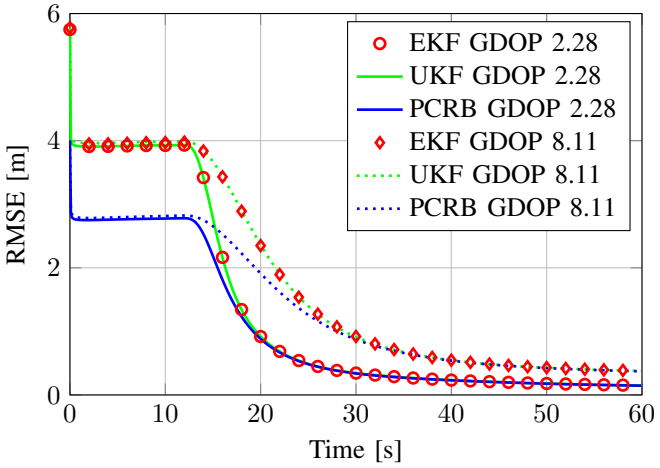

Fig. 1. 1D position RMSE of the **driving** train for **four** visible satellites and the constant velocity scenario.

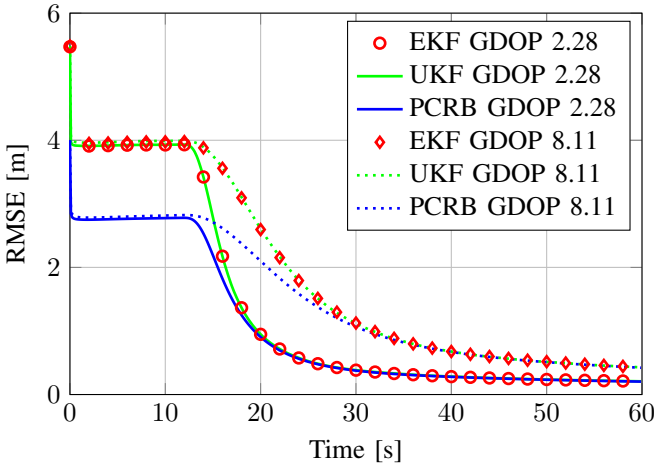

Fig. 2. 1D position RMSE of the **standing** train for **four** visible satellites and the constant velocity scenario.

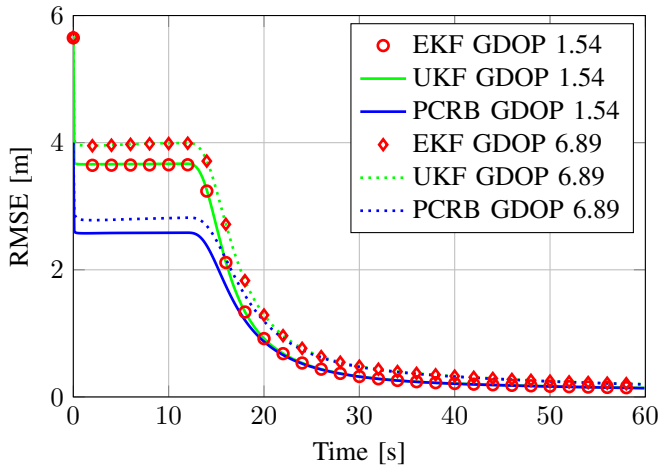

Fig. 3. 1D position RMSE of the **driving** train for **eight** visible satellites and the constant velocity scenario.

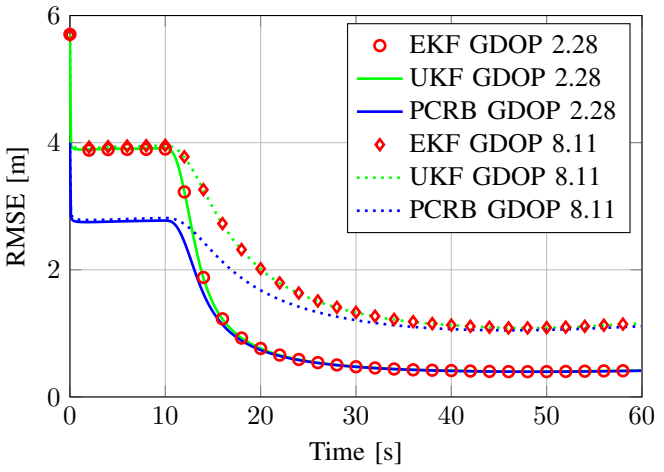

Fig. 4. 1D position RMSE of the train with **constant velocity** for **four** visible satellites and the accelerated scenario.

and 100 realizations of the measurement noise. Therefore the EKF and UKF are evaluated 1×10^5 times in each scenario.

VII. Results

For the scenario where one train is standing and the other moves uniformly, the resulting PCRB and the RMSE of the EKF and UKF for the 1D positions of the trains is shown in Figure 1 and 2 for four visible satellites and two GDOP values. For the EKF, only one in twenty RMSE values is shown to avoid masking the RMSE curve of the UKF. It can clearly be seen in Figure 1 and 2 that the RMSE and the PCRB decay rapidly after approximately 12 s. This is the time when the driving train starts entering the curve. The changing direction and the track constraints are beneficial for estimating the biases on the pseudoranges. The constraints, given in form of the track map, renders it possible to observe the pseudorange bias component perpendicular to the track direction [4]. While driving in the curve, the geometry between satellites and train antenna changes and more parts of the bias can be observed. Because the state space model assumes common pseudorange biases for both trains, this improves also the position estimate of the standing train. The RMSE of both trains therefore has roughly the same value. The comparison of the PCRB and the suboptimal filter, shows a difference of 1.2 m on the straight track and then it converges to the bound while one train is on the curved part of the track. This is true for both GDOP values, but for bigger values the filters converge slower. For the remaining results the RMSE is shown only for one of the trains because the curves are alike.

To get an impression of the dependency of the 1D position accuracy on the number of satellites the RMSE and the PCRB is shown for two constellations with eight satellites in Figure 3 for the driving train. As before, the filters both estimate the position efficiently after the train is in the curved track part. The effect the GDOP has on the RMSE seems to be getting smaller with an increasing number of satellites and the RMSE curves for both values are getting closer together. The reduction of the overall error when more satellites are visible is insignificant. This is not surprising because the 1D position can be determined with only two satellites. In Figure 4 the result of the scenario where the second train is accelerating and approaching the first train in the curve is shown. At the beginning the RMSE behaves like in the example before but after 45 s the PCRB and the RMSE begin to increase. This effect is caused by a decrease in the bias estimation accuracy. When the second train approaches the first train their antenna-satellite geometry is getting more similar. Because only the bias part perpendicular to the driving direction can be observed, the number of observable bias components is reduced and the position RMSE is getting bigger.

VIII. Conclusion

In this paper we proposed a state space model for cooperative localization of trains with GNSS, IMU and a track map. To evaluate the estimation performance of the suboptimal EKF and UKF for this model, a version of the PCRB conditioned on a input vector was derived and it was shown that it is a special case of the hybrid parameter bound. To lower the complexity a recursive version of the bound has been stated and adopted to the concrete state space model. A simulation study has been carried out to show that both filters are able to estimate the 1D position and that the derived PCRB in fact is a lower bound on the RMSE. After an initial phase of larger errors the 1D position RMSE of the filters is close to the PCRB. This improvement is mainly due to the pseudorange bias estimation supported by the changing track geometry and the track constraints.

References

[1] S. Hensel, C. Hasberg, and C. Stiller, "Probabilistic rail vehicle localization with eddy current sensors in topological maps," *IEEE Transactions on Intelligent Transportation Systems*, vol. 12, no. 4, pp. 1525–1536, Dec 2011.

[2] O. Heirich and B. Siebler, "Train-side passive magnetic measurements," in *2015 IEEE International Instrumentation and Measurement Technology Conference (I2MTC) Proceedings*, May 2015, pp. 687–692.

[3] O. Heirich, P. Robertson, and T. Strang, "Railslam-localization of rail vehicles and mapping of geometric railway tracks," in *Robotics and Automation (ICRA), 2013 IEEE International Conference on*. IEEE, 2013, pp. 5212–5219.

[4] P. Zeller, B. Siebler, A. Lehner, and S. Sand, "Relative train localization for cooperative maneuvers using gnss pseudoranges and geometric track information," in *Localization and GNSS (ICL-GNSS), 2015 International Conference on*, June 2015, pp. 1–7.
[5] H. L. Van Trees, *Detection, estimation, and modulation theory*. John Wiley & Sons, 2004.
[6] N. Bergman, "Recursive bayesian estimation," *Department of Electrical Engineering, Linköping University, Linköping Studies in Science and Technology. Doctoral dissertation*, vol. 579, 1999.
[7] H. L. Van Trees, *Bayesian bounds for parameter estimation and nonlinear filtering/tracking*. John Wiley & Sons, 2007.
[8] P. Tichavskỳ, C. H. Muravchik, and A. Nehorai, "Posterior cramér-rao bounds for discrete-time nonlinear filtering," *Signal Processing, IEEE Transactions on*, vol. 46, no. 5, pp. 1386–1396, 1998.
[9] P. W. Bradford, J. Spilker, and P. Enge, "Global positioning system: theory and applications," *AIAA Washington DC*, vol. 109, 1996.